

Calla Lily flower inspired morphing of flat films to conical tubes

Citation for published version (APA):

Peeketi, A. R., Sol, J. A. H. P., Swaminathan, N., Schenning, A. P. H. J., Debije, M. G., & Annabattula, R. K. (2023). Calla Lily flower inspired morphing of flat films to conical tubes. *Journal of Polymer Science*, 61(11), 1065-1073. <https://doi.org/10.1002/pol.20220492>

DOI:

[10.1002/pol.20220492](https://doi.org/10.1002/pol.20220492)

Document status and date:

Published: 01/06/2023

Document Version:

Publisher's PDF, also known as Version of Record (includes final page, issue and volume numbers)

Please check the document version of this publication:

- A submitted manuscript is the version of the article upon submission and before peer-review. There can be important differences between the submitted version and the official published version of record. People interested in the research are advised to contact the author for the final version of the publication, or visit the DOI to the publisher's website.
- The final author version and the galley proof are versions of the publication after peer review.
- The final published version features the final layout of the paper including the volume, issue and page numbers.

[Link to publication](#)

General rights

Copyright and moral rights for the publications made accessible in the public portal are retained by the authors and/or other copyright owners and it is a condition of accessing publications that users recognise and abide by the legal requirements associated with these rights.

- Users may download and print one copy of any publication from the public portal for the purpose of private study or research.
- You may not further distribute the material or use it for any profit-making activity or commercial gain
- You may freely distribute the URL identifying the publication in the public portal.

If the publication is distributed under the terms of Article 25fa of the Dutch Copyright Act, indicated by the "Taverne" license above, please follow below link for the End User Agreement:

www.tue.nl/taverne

Take down policy

If you believe that this document breaches copyright please contact us at:

openaccess@tue.nl

providing details and we will investigate your claim.



World's Most Advanced Photothermal IR Spectroscopy Solutions

Bruker's nanoscale infrared (nanoIR) spectrometers measure spatially varying physical and chemical properties in a diverse range of fields, from polymers and 2D materials to life science and micro-electronics. Fueling an impressive and growing publication record, these systems are advancing academic discovery and helping industrial companies solve critical process problems.

Proprietary spectroscopy and AFM technology:

- **NEW** Dimension IconIR large-sample system with PeakForce property mapping
- High-performance nanoIR spectroscopy with accurate and repeatable FTIR correlation
- Sub-10nm chemical resolution and monolayer sensitivity
- **NEW** Surface Sensitive AFM-IR mode with chemical probing depth to tens of nanometers



Take your materials research to the next level.

Visit www.bruker.com/nanoIR, email productinfo@bruker.com or call +1.408.376.4040/866.262.4040 for more information today.

RESEARCH ARTICLE

Calla Lily flower inspired morphing of flat films to conical tubes

Akhil R. Peeketi¹  | Jeroen A. H. P. Sol²  | Narasimhan Swaminathan¹ |
Albert P. H. J. Schenning^{2,3}  | Micheal G. Debije²  | Ratna K. Annabattula¹ 

¹Center for Responsive Soft Matter, Department of Mechanical Engineering, Indian Institute of Technology Madras, Chennai, India

²Laboratory of Stimuli-Responsive Functional Materials and Devices (SFD), Department of Chemical Engineering and Chemistry, Eindhoven University of Technology (TU/e), Eindhoven, The Netherlands

³Institute for Complex Molecular Systems (ICMS), Eindhoven University of Technology (TU/e), Eindhoven, The Netherlands

Correspondence

Ratna K. Annabattula, Center for Responsive Soft Matter, Department of Mechanical Engineering, Indian Institute of Technology Madras, Chennai 600036, India.

Email: ratna@iitm.ac.in

Micheal G. Debije, Laboratory of Stimuli-Responsive Functional Materials and Devices (SFD), Department of Chemical Engineering and Chemistry, Eindhoven University of Technology (TU/e), 5600 MB, Eindhoven, The Netherlands.

Email: m.g.debije@tue.nl

Funding information

Science and Engineering Research Board, India, Grant/Award Number: CRG/2018/002365; IIT Madras; Ministry of Education, Government of India

Abstract

Recently researchers have developed soft actuators capable of morphing into complex shapes taking inspiration from nature. In this paper, we have developed a splay-nematic liquid crystal polymer network tapered actuator that can morph from a flat film to a cone, mimicking the blooming of single petal Calla Lily flower. We have demonstrated the formation of conical tubes through finite element simulations and experiments. The influence of tapering and alignment orientations with respect to the edge of the film on the cones is analyzed through simulations. The design with tapering and splayed alignments oriented at 45° to the edge is found to be the optimal choice for forming conical tubes.

KEYWORDS

bio-mimicking, calla lilly, cones, liquid crystal polymers, soft actuators

1 | INTRODUCTION

The advent of soft-responsive materials has brought rapid advancements in the field of soft robotics.^{1–5} Motions previously achieved using motors and mechanical actuators are replaced by smart actuators that respond to specific stimuli.^{6–9} Stimuli-responsive actuators like light/heat-responsive liquid crystal polymers, solvent/vapor-responsive hydrogels and heat-responsive shape memory alloys were recently developed.^{4,5,10–25} Inspired by nature, researchers have developed actuators that can perform complex actions using these responsive systems. Actuators which mimic

the blooming of flowers,^{26–30} motion of caterpillars,^{31–33} trapping of flies like Venus flytrap⁶ and tight rolling of proboscis of butterfly,^{34,35} among others, were developed.

Having the stimuli-responsive films mimic the blooming of flowers is one of the popular ways to show the versatility of actuation in the responsive systems.^{26–30} The majority of such systems deploy the responsive thin films radially as petals and the blooming of flower comes from bending/unbending of these artificial petals. However, such simple bending actuations will not be able to reproduce blooming of flowers that have a single petal such as the Calla Lily. The Calla Lily flower initially

This is an open access article under the terms of the [Creative Commons Attribution-NonCommercial](https://creativecommons.org/licenses/by-nc/4.0/) License, which permits use, distribution and reproduction in any medium, provided the original work is properly cited and is not used for commercial purposes.

© 2022 The Authors. *Journal of Polymer Science* published by Wiley Periodicals LLC.

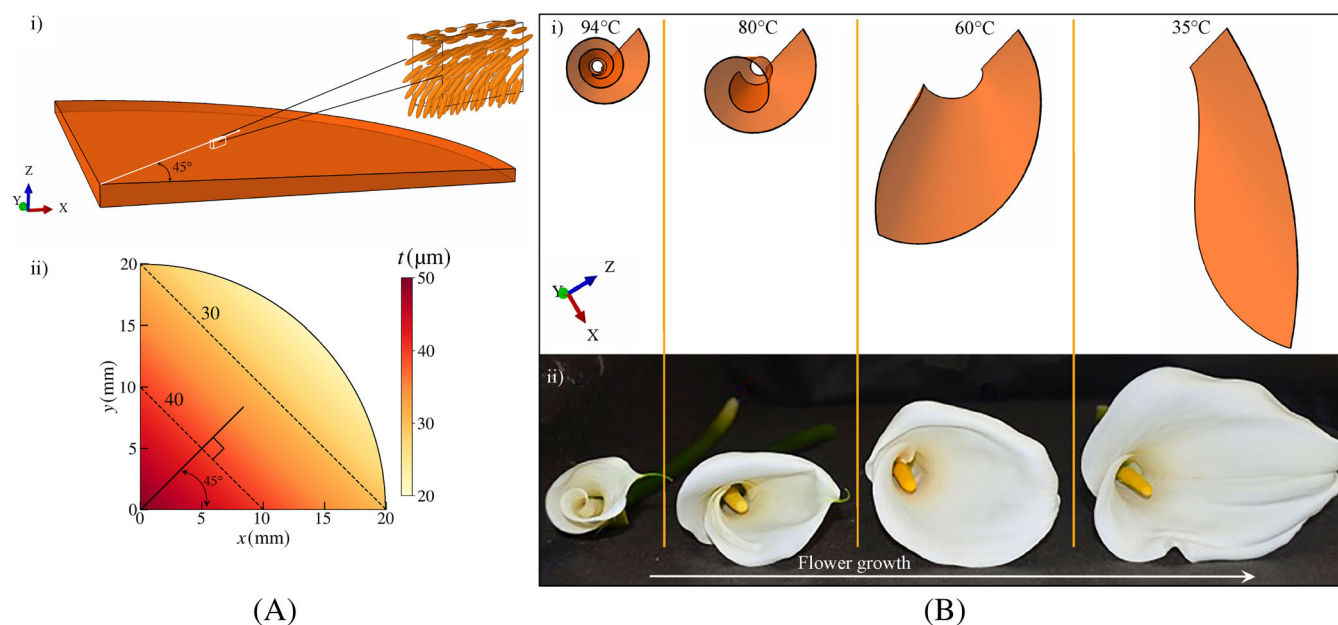


FIGURE 1 (A) Schematic illustration of the designed LCN actuator with both (i) splayed alignment (inset shows the alignment of mesogens through the depth) and (ii) tapered thickness (the color bar indicates the thickness in μm and the dashed lines represent the isocountours of thickness) oriented at 45° to the edge. (B-i) Finite element simulation snapshots (at different temperatures) of thermally actuated rolling of a quarter circular soft actuator into a conical tube mimicking the Calla Lily flower. (B-ii) Snapshots of Calla Lily flower showing the blooming from conical tubes to flat petal. Figure B-ii is reproduced from reference 36. Copyright 2015 Authors, licensed under a Creative Commons Attribution (CC BY) license.

begins as a conical tube, which then blooms to a wider petal.³⁶ Among responsive systems, liquid crystal based polymers attract special attention as deformations can be programmed through specific alignment of liquid crystal mesogens. Depending on the local alignment of the mesogens, the initially flat films can either remain flat or morph into different shapes, such as curls, twists, and cones.^{4,37} Moreover, the low viscous liquid crystal mixture enables fabricating thin films of desired thicknesses with ease. The anisotropic nature of the liquid crystal mesogens carries over to the crosslinked polymer film, which feature strongly anisotropic mechanical and optical properties. This anisotropic nature coupled with ease of local alignment control enables LCNs to show complex deformation modes.

In one of our earlier works, we demonstrated how a tapered splayed actuator can bend through several hundred degrees resulting in multiple rolls.³⁴ In this work, we use the idea of tapering induced rolling to design a liquid crystal polymer network (LCN) film that can mimic the blooming of Calla Lily flower as demonstrated in Figure 1. The designed LCN actuator has both splayed alignment and tapering aligned at 45° to an edge of the film (see Figure 1A) in contrast to our earlier work where the tapering and alignment are parallel to one of the edges. Previous works which demonstrated formation of cones through liquid crystal polymer films used azimuthal alignments fabricated using

sophisticated photo-alignment setups.^{38,39} In this work, the cones arise from a combination of tapered thickness, boundary condition and direction of uniform splayed alignment. Finite element simulations were performed to determine the optimal choice of alignment and taper directions for forming cones. Moreover, we have also demonstrated the formation of cones through experiments. The details of the computational model and experiments are presented in Section 2. The choice of tapering direction along with the direction of splayed alignment that decides the geometry of the final configuration are discussed in Section 3.

2 | METHODS

2.1 | Computational modeling

The thermo-mechanical response of the tapered LCN actuator and its final shape are determined through a one-way coupled thermo-mechanical model simulated using the commercial finite element software, Abaqus.⁴⁰ Square films of size, $\ell = 10$ mm with different orientations of splayed alignment and tapering with respect to an edge are used for simulations. The values of orientation direction (direction of planar mesogens in the splayed alignment), α , and tapering direction, β , schematically illustrated in Figure 2, are varied to study their

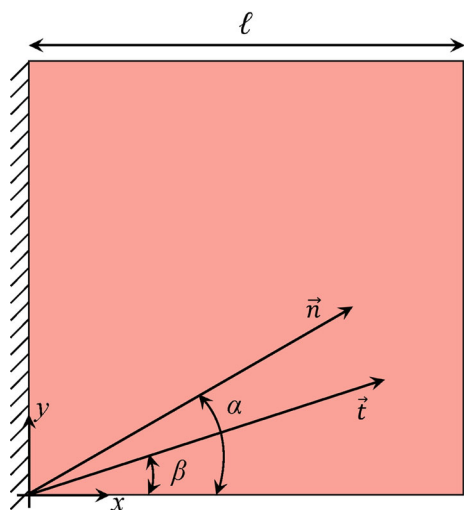


FIGURE 2 Schematic illustration of the square film used in finite element simulations depicting the orientation of the splayed alignment (α) and the tapering (β) with respect to the bottom edge along with identification of the fixed edge (left) of the film.

influence on the formation of cones. The local thickness of the film is determined in terms of β as,

$$t(x, y) = t_0 - \Delta t \frac{x + y \tan \beta}{\ell(1 + \tan \beta)}, \quad (2.1)$$

where t_0 and Δt are taken as 50 and 30 μm , respectively. The edge $x = 0$ of the film is fixed in the simulations. The finite element simulations are performed using a mesh size of 0.1 mm. The film configuration is defined in terms of the displacement, \mathbf{u} , from the initial flat film.

The total Lagrangian strain (\mathbf{E}) in terms of the unknown displacements (\mathbf{u}) is,

$$\mathbf{E} = \frac{(\nabla \mathbf{u} + \nabla \mathbf{u}^\top + \nabla \mathbf{u}^\top \nabla \mathbf{u})}{2}, \quad (2.2)$$

where $()^\top$ indicates the transpose. The finite thermo-mechanical strain (\mathbf{E}^{th}) due to the rise in temperature may be written as,

$$\mathbf{E}^{\text{th}} = \Delta T \mathbf{R}, \quad (2.3)$$

where \mathbf{R} is the thermal expansion tensor and ΔT is the temperature change. Now, the stress tensor, \mathbf{S} , can be estimated in terms of \mathbf{E} and \mathbf{E}^{th} as,

$$\mathbf{S} = \mathbf{C} : \mathbf{E} - \mathbf{C} : \mathbf{E}^{\text{th}}, \quad (2.4)$$

where \mathbf{C} is the fourth-order elastic moduli tensor. Solving for the mechanical equilibrium ($\nabla \cdot \mathbf{S} = 0$) through quasi-

static solution procedure gives the unknown displacements, \mathbf{u} , and thus the final configuration of the film.

The variations in the alignment through the depth of the film are implemented using composite shell elements (S4R). The alignment is varied linearly through the thickness in 91 discrete steps from planar (0°) at the top face to homeotropic (90°) at the bottom face. The elastic moduli tensor, \mathbf{C} , is estimated using the moduli reported by Sol et al.³⁴ along the parallel E_{\parallel} and perpendicular E_{\perp} directions to the director and a Poisson's ratio of 0.3 for $\nu_{\parallel, \perp}$ and $\nu_{\perp, \perp}$ (isotropic plane). As the shear modulus is not available, the value for shear modulus $G_{\parallel, \perp}$ is assumed to be $E_{\parallel}/(2[1 + \nu_{\parallel, \perp}])$ and $G_{\perp, \perp}$ to be $E_{\perp}/(2[1 + \nu_{\perp, \perp}])$. Note that the elastic moduli are expected to have negligible effects on the final shape, as the deformation is spontaneous. The elements of the elasticity tensor (\mathbf{C}) for each layer of the splay alignment are estimated using the appropriate rotational transformation. The thermal expansion tensor (\mathbf{R}) is also estimated from the coefficient of thermal expansions in the directions parallel and perpendicular to the director orientation provided by Sol et al.³⁴

2.2 | Experiments

2.2.1 | Preparation of LC mixture

The experimental procedure is based on the work published by Sol et al.³⁴ In short, 4-methoxyphenyl-4-(6-acryloyloxy hexyloxy) benzoate (**1**) and 1,4-di(4-(6-acryloyloxy hexyloxy) benzoyloxy)-2-methylbenzene (**2**) (both obtained from Merck KGaA), make up 98 wt% in the total mix. 1 wt% of reactive photoresponsive dye *N*-ethyl-*N*-(2-hydroxyethyl)-4-(4-nitrophenylazo)aniline is added (**3**, obtained from Sigma-Aldrich). Finally, 1 wt% of free radical photo initiator bis(2,4,6-trimethylbenzoyl)phenyl phosphine oxide is added (**4**, obtained from Sigma-Aldrich). Figure 3 shows the molecular structures of the above-mentioned materials. To the solid mix, dichloromethane (CH_2Cl_2 , obtained from Biosolve) is added to allow for proper mixing for about 30 min. The vial is then moved to a hot plate at 80°C where it remains overnight, and after this, a few hours in a vacuum oven at room temperature. At this point, near-complete removal of the solvent is assumed.

2.2.2 | Preparation of wedge-shaped LC alignment cells

A $3 \times 3 \text{ cm}^2$ borosilicate glass slides are sonicated (Branson 2510) for 20 min in a mixture of 1:1 v/v ethanol-isopropanol. Subsequently, the glass slides are blown dry under an N_2 flow and placed in a UV/ O_3 oven

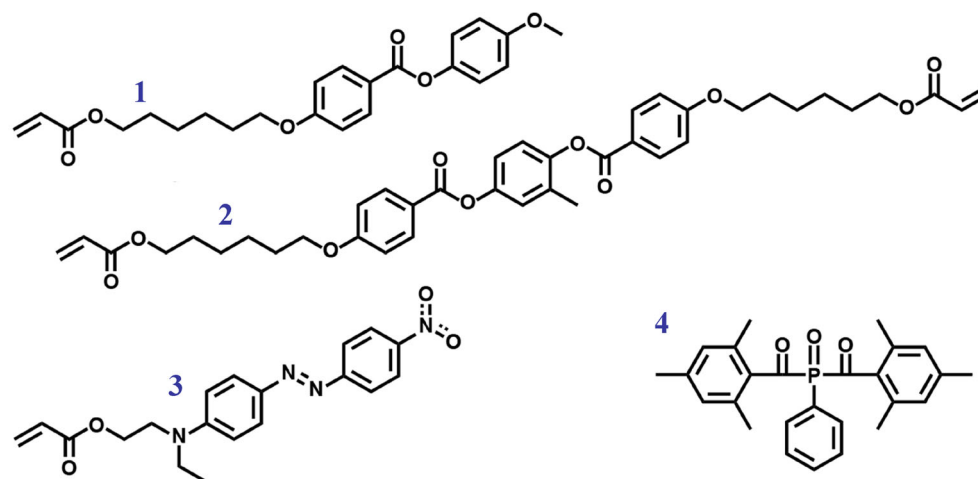


FIGURE 3 Components of the LC mixture: (1) 4-methoxyphenyl-4-(6-acryloyloxy hexyloxy)benzoate; (2) 1,4-di(4-(6-acryloyloxy hexyloxy)benzoyloxy)-2-methylbenzene; (3) *N*-ethyl-*N*-(2-hydroxyethyl)-4-(4-nitrophenylazo)aniline; (4) bis(2,4,6-trimethylbenzoyl)phenyl phosphine oxide.

(UV Products PR-100) for 20 min to activate the glass's surface. Then, a polyimide (PI) precursor is spin coated (5 s at 800 rpm followed by 45 s at 5000 rpm). For planar alignment Optmer AL1051 (JSR Corp.) is used. Sunever 5661 (Nissan Chemical Corp.) is used for homeotropic alignment. Two curing steps follow: ≈ 10 min at 90°C , after which the slides are baked 90 min at 180°C . Uniaxial planar alignment is induced by rubbing PI-coated slides on a velvet cloth. Wedge-shaped, splay-aligned cells are made by gluing planar- and homeotropic-aligned glass slides together with coated sides facing each other. Depending on the spacing thickness required, different techniques are used: (i) for 10, 20, 30 μm : to a UV-curable resin (Norland UV Sealant 91), 1% w/w of polymer beads (Sekisui Micropearl SP) of the demanded size is mixed through the resin, and (ii) for 50 μm : double-sided tape of 50 μm thickness is employed. The selected combination of adhesives are applied on one side of the cell, the other glass slide is placed on top. Paper clamps are used to hold the glass slides together during UV-curing of the glue. Quality of the wedge-shape is judged by visually examining the sample for a lamellar-shaped optical interference fringe pattern when the cell is viewed under a bright light source.

2.2.3 | Fabrication of the LCNs

Wedge-shaped cells were filled with the liquid crystal mixture at 85°C through capillary action. After cooling down to 55°C (to the nematic phase of the LC mix), a UV flood exposure is initiated and maintained at $\approx 10 \text{ mWcm}^{-2}$ for 900 s (EXFO Omnicure S2000) to facilitate free radical polymerization. A post-curing step of 20–30 min on a 120°C hot plate is done to ensure maximum conversion and remove shrinkage-related stresses after polymerization. Cells are opened, and samples of

specific shapes are cut from the square polymer films for analysis.

2.2.4 | Analysis of thermo-mechanical behavior

The cut samples are placed in an oven with appropriate arrangements that allows for filming the deformation as the environment heats up. The temperature is recorded using a digital sensor (Sensirion SHT3x), and photographs are taken with a digital camera (Olympus OM-D E-M10 Mk III, M.Zuiko 60 mm f/2.8 lens) in manual mode.

The reader may refer to Sol et al.³⁴ for the detailed chemical and physical characterizations such as differential scanning calorimetry, FT-IR spectra, scanning electron micrograph of the film highlighting the alignment of mesogens through the depth of the film, dynamic mechanical analysis and thermal expansion of the films.

3 | RESULTS AND DISCUSSION

Upon heating, the order of the nematic liquid crystal mesogens decreases resulting in a contraction of the LCN in the direction parallel to the alignment and an expansion in the perpendicular direction. The spontaneous thermal strain as a function of temperature in both the directions is plotted in Figure 4A. The principle curvature of bending increases with the decrease in the thickness as seen in Figure 4B independent of the orientation of the splayed alignment when only a corner point of the film is fixed. The axis of bending is always perpendicular to the splayed alignment direction as can be noticed from insets in Figure 4B. Here, the corner is fixed to replicate the free unconstrained bending of the films. In the following, we introduce a thickness tapering of the film and an

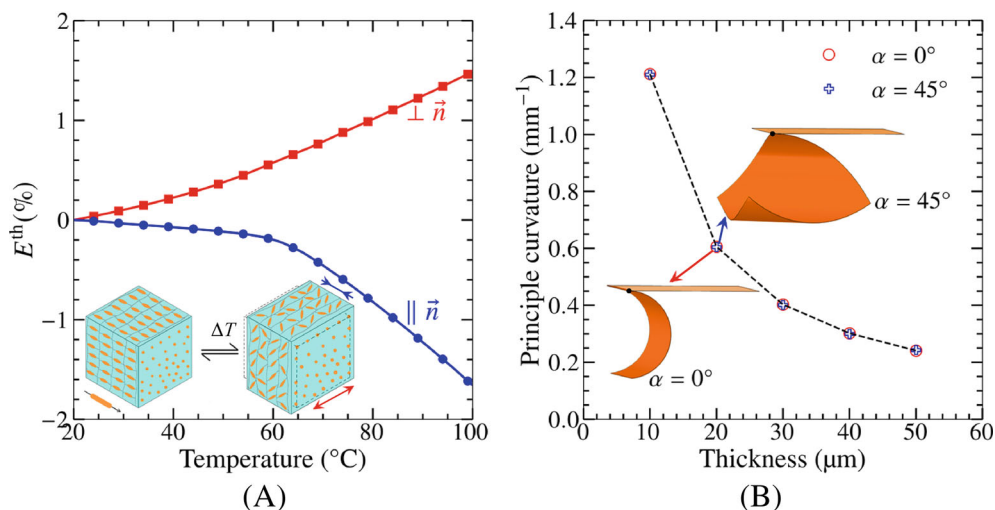


FIGURE 4 (A) The transversely isotropic thermal strain in the directions parallel and perpendicular to the alignment of the LCN (inset highlights the heating induced “order–disorder transition” that results in spontaneous transversely isotropic strains). (B) Influence of the thickness and the splayed alignment orientation direction (α) on the principle curvatures attained by heating the initially flat films of size 5 mm and of uniform thickness to a temperature of 65°C. (Inset on the left bottom shows the bending of the 20 μm film with splayed alignment along the edge and the inset on the right top corresponds to the 20 μm film with splayed alignment oriented at 45° with the edge. The black dot highlighted on the films indicate the fixed boundary condition.)

appropriate boundary constraint to demonstrate the formation of cones as opposed to the uniform rolls as discussed above.

The choice of orientation direction (direction of planar mesogens in the splayed alignment), α , and tapering direction, β , (see Figure 2) determines the formation of cones. The films are fixed on their left edge along the Y-axis. The film rolls with multiple turns similar to the proboscis of a butterfly for the case when orientation and tapering are along the X-axis ($\alpha = 0$, $\beta = 0$) as shown in Figure 5A similar to Sol et al.³⁴ Since the splayed alignment is oriented along x-axis, the principle curvature is independent of y (far away from the edge) and increases along the x-axis following the tapering in thickness forming a cylindrical structure. In order to mimic the Calla Lily flower, curvature of the roll should also vary along the width, giving rise to a conical shape. For $\alpha = 45^\circ$ and $\beta = 0$, a varying curvature along the x and y-axis is generated forming the cone (see Figure 5B). Furthermore, the case of splayed alignment and taper along the diagonal of the film ($\alpha = \beta = 45^\circ$) also actuates to a cone as seen in Figure 5C. The local principle curvature mapped to the initial flat film shown in the bottom row of Figure 5 illustrates that the curvatures look similar for the cases $\alpha = 45^\circ$, $\beta = 0^\circ$ and $\alpha = \beta = 45^\circ$. In the absence of fixed boundary at the left edge (see Figure 2), the film rolls similarly to the case with tapering and alignment along the X-axis ($\alpha = \beta = 0^\circ$) but with rolling direction along the diagonal (as also seen in Figure 4B for films

of uniform thickness). The fixed boundary along the Y-axis constrains the nearby region and thus creating a cone as seen in Figures 1B and 5. The evolution of a quarter circular actuator of $\alpha = \beta = 45^\circ$ with the increase in temperature is shown in Figure 1B, comparing with the growth of the Calla Lily flower. The actuator deforms from a flat shape to conical shape with the increase in temperature.

Finite element simulations (see Section 2.1) have been carried out with different choices for taper and alignment directions to investigate the formation of cones and determine the optimal choice for forming cones. To characterize the cones, cone angle defined as the angle between the fixed edge and axis of the formed cone as indicated in Figure 6A is used. Cone angle indicates the deviation of the cone from the ideal cylinder. The axis of the cone is estimated using principle component analysis (PCA) of the nodal coordinates of the meshed cone. PCA gives the dominant vectors for the input data and for a cone, one of the vectors correspond to its axis. Cone angle (θ) can then be estimated from the axis, \vec{a} and fixed edge, \vec{f} as

$$\theta = \cos^{-1} \left(\frac{\vec{f} \cdot \vec{a}}{|\vec{f}| |\vec{a}|} \right). \quad (3.1)$$

Figure 6B shows the variation of cone angle with alignment direction and taper direction when films are heated from room temperature (initial flat shape) to 90°C

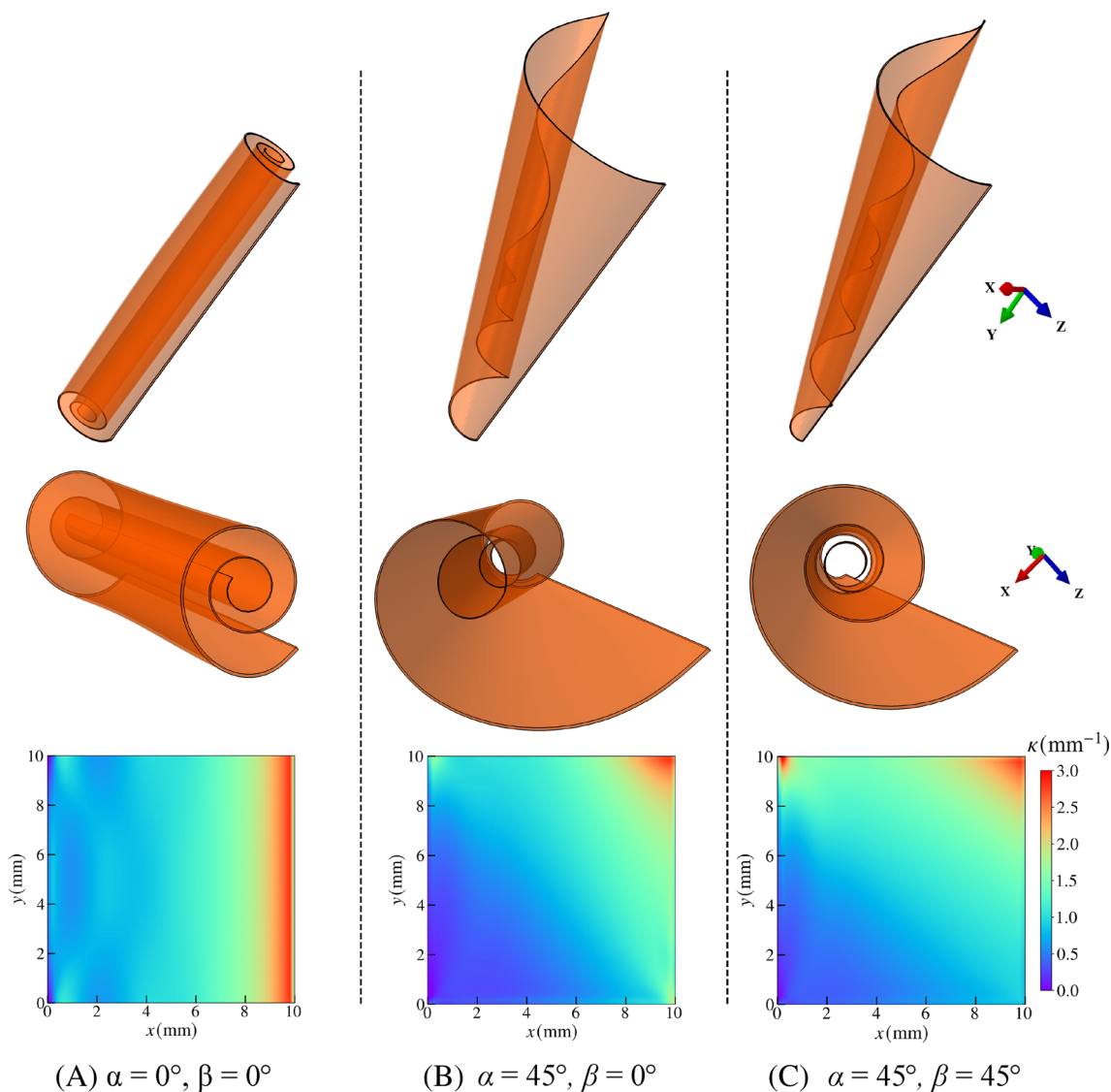


FIGURE 5 Finite element simulation snapshots of thermo-actuated rolling of a square film heated to 100 from 19°C (flat shape) with different values for the orientation of the splayed alignment and the taper. The bottom row shows the local principle curvature (κ) mapped to the initial flat film for each case.

(cone shape). It can be noticed that the alignment direction (α) strongly influences the cone angle while the tapering direction (β) has weak influence. $\alpha = 45^\circ$, $\beta = 0^\circ$ has higher cone angle than the case of $\alpha = \beta = 45^\circ$ even though latter seems to have formed a more compact cone (see Figure 5B,C). To quantify the quality of the cone formed, variance of the cone is used in addition to the cone angle. The variance (σ^2) is estimated from the nodal coordinates of the cone as,

$$\sigma^2 = \frac{\sum (r_i - \bar{r})^2}{n}, \quad (3.2)$$

where r_i is the shortest distance of node i from the axis of the cone, \bar{r} is the mean of shortest distances from axis

($= \frac{\sum r_i}{n}$) and n corresponds to total number of nodes. The variance is plotted in Figure 6C for different values of α and β . It can be noticed that σ^2 is lower for $\alpha = \beta = 45^\circ$ than that of $\alpha = 45^\circ$, $\beta = 0^\circ$ indicating that the former is compact. The best quality cones will have higher cone angle but least variance. Hence, $\alpha = \beta = 45^\circ$ is the optimal choice for forming cones from LCNs.

We have also fabricated a liquid crystal polymer network film with the alignment along the diagonal and different spacers at the 4 corners to create tapered thickness (see Figure 7A). The film is actuated in an oven where it rolled into cone as seen in Figure 7B. The tapered diameter of the folded configuration can be noticed from the experimental snapshots indicating a

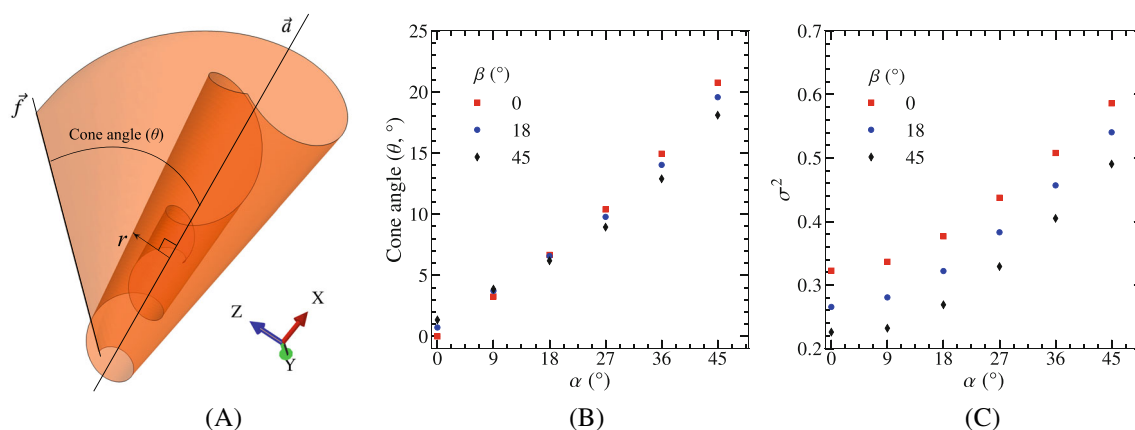


FIGURE 6 (A) Schematic illustration of the cone angle (θ) defined as the angle between the fixed edge (f) and the axis of the cone (a), and the shortest distance (r) from a node of cone to its axis. Influence of orientation direction (α) and tapering direction (β) on the (B) cone angle (θ) and the (C) variance (σ^2) for films heated from initially flat shape at 19 to 90°C.

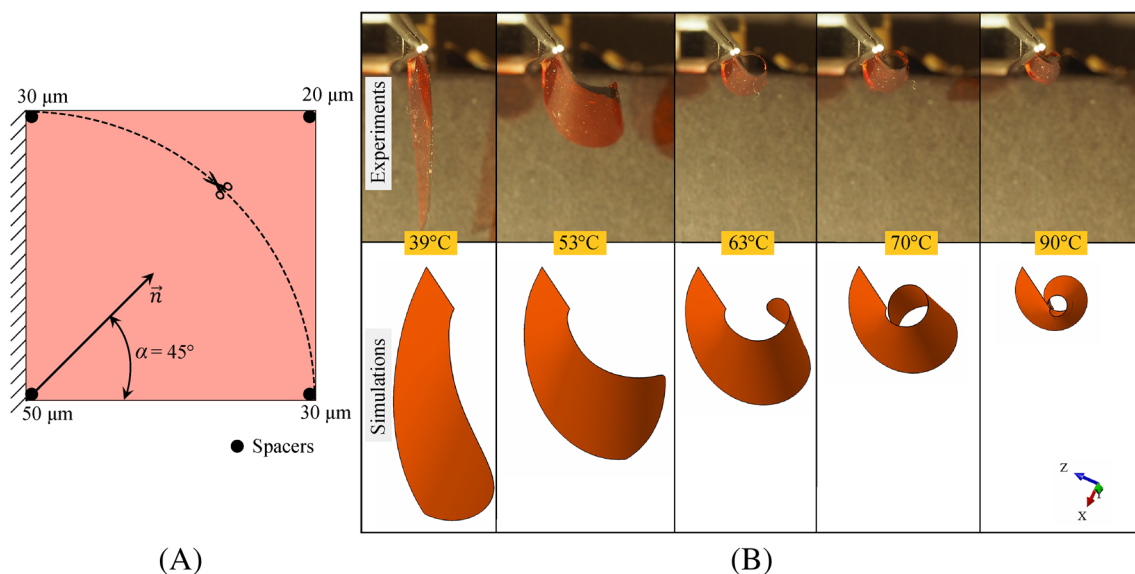


FIGURE 7 (A) Schematic depicting the spacers used at the corners for creating varying thickness in the liquid crystal polymer film and indicating the cut made in the sample to make a quarter circular film. (B) Comparison of the thermal-induced formation of conical tube from a quarter circular tapered splayed liquid crystal polymer network film through experiments and simulations.

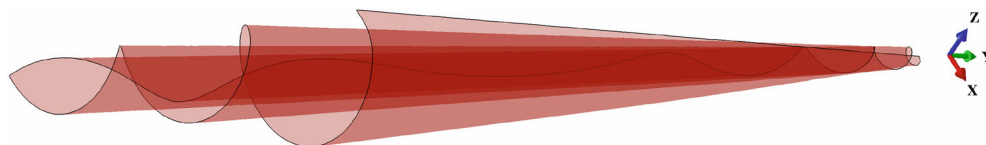


FIGURE 8 A tight conical tube generated from a quarter circular tapered actuator with $\alpha = \beta = 45^\circ$ and thickness tapering from 20 to 10 μm when heated to 75°C.

conical shape. The corresponding finite element simulation snapshots are also shown for comparison. The thickness of the film in simulations is calculated using $t = 0.05 - 0.02 \frac{x+y}{20}$ mm to be close to experimental thickness distribution. The differences in the simulation and

experiments may be due to the pre-bent of the fabricated films at room temperature.

Conical tubes made of Platinum in H_2O_2 solution have been shown to act as catalytic micro jet engines.^{41,42} The LCN conical tubes shown in this work can be coated

with required material to work as a micro jet under a specific solution environment. One major advantage of using LC systems for such an application is that an initially flat film under the application of an external stimulus such as light or heat can be morphed into a tight conical tube (see Figure 8) that can act as a micro jet providing on-demand propulsion.

4 | CONCLUSIONS

In summary, we have simulated and experimentally demonstrated the formation of a cone from flat soft actuator, mimicking the blooming of single petal flowers. By varying the alignment and taper directions from being parallel to the one of the edges of a square film to being parallel to the diagonal resulted in the formation of cones. Finite element simulations showed that the cone angle increased with increase in the deviation of the alignment direction from parallel to the edge. The tapering direction had least influence on the cone angles. The formation of tight conical tubes from flat structures could have potential applications as on-demand conical micro jets.

ACKNOWLEDGMENTS

Ratna K. Annabattula gratefully acknowledges the financial support from Science and Engineering Research Board, India, through a core research grant CRG/2018/002365. Akhil R. Peeketi acknowledges the financial support through Prime Minister's Research Fellowship for conducting doctoral research at IIT Madras. We acknowledge the generous financial support from IIT Madras under the institutes of eminence (IoE) scheme funded by Ministry of Education, Government of India. The authors acknowledge the use of the computing resources at HPCE, IIT Madras.

CONFLICT OF INTEREST


The authors declare that they have no conflict of interest.

DATA AVAILABILITY STATEMENT

Data sharing is not applicable to this article as no new data were created or analyzed in this study.

ORCID

Akhil R. Peeketi  <https://orcid.org/0000-0002-9955-7129>

Jeroen A. H. P. Sol  <https://orcid.org/0000-0002-1666-8502>

Albert P. H. J. Schenning  <https://orcid.org/0000-0002-3485-1984>

Micheal G. Debije  <https://orcid.org/0000-0001-8844-1115>

Ratna K. Annabattula  <https://orcid.org/0000-0002-9492-8592>

REFERENCES

- [1] L. Ionov, *Polym. Rev.* **2013**, *53*, 92.
- [2] E. M. White, J. Yatvin, J. B. Grubbs III, J. A. Bilbrey, J. Locklin, *J. Polym. Sci., Part B: Polym. Phys.* **2013**, *51*, 1084.
- [3] C. Yoon, *Nano Converg* **2019**, *6*, 1.
- [4] K. Mehta, A. R. Peeketi, L. Liu, D. Broer, P. Onck, R. K. Annabattula, *Appl Phys Rev* **2020**, *7*, 041306.
- [5] M. Pilz da Cunha, M. G. Debije, A. P. H. J. Schenning, *Chem. Soc. Rev.* **2020**, *49*, 6568.
- [6] O. M. Wani, H. Zeng, A. Priimagi, *Nat. Commun.* **2017**, *8*, 1.
- [7] M. Pilz da Cunha, A. R. Peeketi, K. Mehta, D. J. Broer, R. K. Annabattula, A. P. Schenning, M. G. Debije, *Chem. Commun.* **2019**, *55*, 11029.
- [8] A. Ramgopal, A. R. Peeketi, R. K. Annabattula, *Soft Matter* **2021**, *17*, 7714.
- [9] M. Babaei, J. Gao, A. Clement, K. Dayal, M. R. Shankar, *Soft Matter* **2021**, *17*, 1258.
- [10] I. Tokarev, S. Minko, *Soft Matter* **2009**, *5*, 511.
- [11] H. Meng, J. Hu, *J. Intell. Mater. Syst. Struct.* **2010**, *21*, 859.
- [12] L. Sun, W. M. Huang, Z. Ding, Y. Zhao, C. C. Wang, H. Purnawali, C. Tang, *Mater. Des.* **2012**, *33*, 577.
- [13] C. P. Ambulo, J. J. Burroughs, J. M. Boothby, H. Kim, M. R. Shankar, T. H. Ware, *ACS Appl. Mater. Interfaces* **2017**, *9*, 37332.
- [14] T. J. White, *J. Polym. Sci., Part B: Polym. Phys.* **2018**, *56*, 695.
- [15] Leeladhar, P. Raturi, J. P. Singh, *Sci. Rep.* **2018**, *8*, 1.
- [16] R. Samanta, S. Ghosh, R. Devarapalli, C. M. Reddy, *Chem. Mater.* **2018**, *30*, 577.
- [17] X. Peng, H. Wang, *J. Polym. Sci., Part B: Polym. Phys.* **2018**, *56*, 1314.
- [18] M. Tabrizi, T. H. Ware, M. R. Shankar, *ACS Appl. Mater. Interfaces* **2019**, *11*, 28236.
- [19] J. Singh et al., *Sens. Actuators, A* **2019**, *296*, 87.
- [20] P.-F. Luo, S.-L. Xiang, C. Li, M.-Q. Zhu, *J Polym Sci* **2021**, *59*, 2246.
- [21] R. K. Meena, S. D. Rapaka, R. Pratoori, R. K. Annabattula, P. Ghosh, *Soft Matter* **2022**, *18*, 372.
- [22] M. Ganesan, R. Kumar, D. K. Satapathy, *Langmuir* **2022**, *38*, 6066.
- [23] G. Manikandan, A. Murali, R. Kumar, D. K. Satapathy, *ACS Appl. Mater. Interfaces* **2021**, *13*, 8880.
- [24] D. Jayoti, A. R. Peeketi, R. K. Annabattula, S. K. Prasad, *Soft Matter* **2022**, *18*, 3358.
- [25] P. Satapathy, R. Adiga, M. Kumar, G. Hegde, S. K. Prasad, *J Nanostructure Chem* **2022**, *12*, 235.
- [26] C. Yao, Z. Liu, C. Yang, W. Wang, X.-J. Ju, R. Xie, L.-Y. Chu, *Adv. Funct. Mater.* **2015**, *25*, 2980.
- [27] A. Rath, P. Geethu, S. Mathesan, D. K. Satapathy, P. Ghosh, *Soft Matter* **2018**, *14*, 1672.
- [28] Y. Wang, W. Huang, Y. Wang, X. Mu, S. Ling, H. Yu, W. Chen, C. Guo, M. C. Watson, Y. Yu, L. D. Black III, M. Li, F. G. Omenetto, C. Li, D. L. Kaplan, *Proc Natl Acad Sci* **2020**, *117*, 14602.
- [29] S.-L. Xiang, Y.-X. Su, H. Yin, C. Li, M.-Q. Zhu, *Nano Energy* **2021**, *85*, 105965.
- [30] Y. Pan, L. H. Lee, Z. Yang, S. U. Hassan, H. C. Shum, *Nano-scale* **2021**, *13*, 18967.
- [31] H. Okuzaki, T. Saido, H. Suzuki, Y. Hara, H. Yan, *J. Phys. Conf. Ser.* **2008**, *127*, 012001.

- [32] J.-S. Koh, K.-J. Cho, in *2009 IEEE International Conference on Robotics and Biomimetics (ROBIO)*, IEEE, **2009**, pp. 1154–1159.
- [33] H. Zeng, O. M. Wani, P. Wasylczyk, A. Priimagi, *Macromol. Rapid Commun.* **2018**, *39*, 1700224.
- [34] J. A. H. P. Sol, A. R. Peeketi, N. Vyas, A. P. H. J. Schenning, R. K. Annabattula, M. G. Debije, *Chem. Commun.* **2019**, *55*, 1726.
- [35] A. Potekhina, C. Wang, *Appl. Phys. Lett.* **2021**, *118*, 241903.
- [36] T. S. Sales, P. D. de Oliveira Paiva, G. M. Manfredini, Á. M. P. Nascimento, M. L. R. Castro, *Ornamental Horticulture* **2015**, *21*, 368.
- [37] T. J. White, D. J. Broer, *Nat. Mater.* **2015**, *14*, 1087.
- [38] L. T. de Haan, C. Sánchez-Somolinos, C. W. M. Bastiaansen, A. P. H. J. Schenning, D. J. Broer, *Am. Ethnol.* **2012**, *124*, 12637.
- [39] T. H. Ware, M. E. McConney, J. J. Wie, V. P. Tondiglia, T. J. White, *Science* **2015**, *347*, 982.
- [40] M. Smith, *ABAQUS/Standard User's Manual, Version 6.9*, Dassault Systèmes Simulia Corp, Providence, RI, USA, **2009**.
- [41] W. Gao, S. Sattayasamitsathit, J. Orozco, J. Wang, *J. Am. Chem. Soc.* **2011**, *133*, 11862.
- [42] V. M. Fomin, M. Hippler, V. Magdanz, L. Soler, S. Sanchez, O. G. Schmidt, *IEEE Trans Robot* **2013**, *30*, 40.

How to cite this article: A. R. Peeketi, J. A. H. P. Sol, N. Swaminathan, A. P. H. J. Schenning, M. G. Debije, R. K. Annabattula, *J. Polym. Sci.* **2023**, *61*(11), 1065. <https://doi.org/10.1002/pol.20220492>